Original Research Article

Estimation of Regional Evapotranspiration based on Tri-Angle Method Using Thermal and VNIR Data.

Abstract

Evapotranspiration is a critical component in the hydrological cycle, water resources management and climate studies especially in arid and semi-arid regions. This paper aimed at producing a simplified and applicable procedure for estimating spatial distributed daily actual evapotranspiration (ET_a) directly at regional scale using thermal and visible-near infra-red (VNIR) data. The findings of this study will be useful for irrigation water management, climate change studies and water resources planning in the study region. Triangle method, which makes a parameterization of priestly-Taylor equation, was used to estimate ET_a at daily scale directly by using a simplified approach with realistic hypotheses. This study conducted in Egypt, Salhia, 6th of October Company as an arid region over the winter crops (wheat, potato and sugar beet) cultivated there using multi date Landsat images. The results were compared with ET_a values adjusted from crop evapotranspiration ET_c "FAO Penmamn-Monteith approach" using the Crop Water Stress Index (*CWSI*). The results showed high accuracy and good agreement against assessment method. The correlation factor (R^2) values for wheat, potato and sugar beet were 0.88, 0.98 and 0.99 and Root Mean Square Error (RMSE) were 0.2, 0.26 and 0.37 respectively over the different dates. In the 16th of April, 2014 there was a significant difference in wheat curves as the RMSE were 0.8 and we explained the reasons of this difference as it is a result of the sprinkler irrigation system effect on the mature wheat. This results show that the proposed procedure is accurate enough at least in most cases of our study for estimating the regional surface ET_a but it need to evaluate for wheat under other irrigation systems like surface or drip irrigation systems .

Keywords: Remote sensing, *ETa*, Landsat, CWSI and Arid regions.

1. Introduction

Fresh water resources are becoming increasingly limited in many parts of the world, and decision makers are demanding new tools for monitoring water availability and rates of consumption [26]. The water shortage is the main constraint and a major limiting factor facing the implementation of the country's future economic development plans [27]. Global estimates of water consumption by sector indicate that irrigated agriculture is responsible for 85% of the water-use and that consumption in this sector will increase by 20% by 2025 [10]. In general, water availability is a major limitation for crop production and agriculture development specially, in arid and semi-arid regions. Egypt is under the water poverty line, as the per capita is less than 650 m^3/year. In addition to water poverty, Egypt faces a great danger due to the millennium dam in Ethiopian, which will lead to water quota shortage from the Nile River. As the agriculture sector is the largest consumer of fresh water, so it will be the first and largest sector influenced by this shortage. Management water resources, developing irrigation systems and actual water requirements studies must be conduct in order to face this danger. A better understanding of the water balance is essential for exploring water saving techniques. One of the most important

43 concepts regarding water balance in arid and semi-arid areas is crop evapotranspiration (*ETc*)
44 which is a key factor for determining proper irrigation scheduling and for improving water use
45 efficiency in irrigated agriculture [11-41]. Large volumes of water transfer from the soil and
46 vegetation to atmosphere by evapotranspiration (*ET*). Accurate, spatially distributed information
47 on water use, quantified at the scale of human influence, has been a long-standing critical need
48 for a wide range of applications. Quantifying *ET* for irrigated crops in arid regions is vital to
49 water resources management. The detailed *ET* maps enable managers to allocate available water
50 precisely among agricultural, urban, and environmental uses. The actual rate of water use by
51 vegetation can deviate significantly from potential *ET* rates due to impacts of drought, disease,
52 insects, vegetation amount, phenology, soil texture, fertility and salinity [1-2-26]. Different
53 methods have been proposed for measuring *ET* on various spatial scales from individual plants to
54 fields or landscape scales. However, conventional techniques provide essentially point
55 measurements, which usually do not represent areal means because of the heterogeneity of land
56 surfaces and the dynamic nature of heat transfer processes [39-40]. In recent years, as a result of
57 the enormous developments in remote sensing technology, satellite data specifications, spatial,
58 temporal and spectral resolution, are continuously improving. Many surface parameters, such as
59 albedo, vegetation coverage, land surface temperature, and leaf area index, can be retrieved from
60 visible, near-infrared, thermal infrared and other bands of satellite data. These data provide a
61 basis for estimating *ET* from farmland and other regions and have attracted widespread attention
62 for the use of remote sensing technologies to study regional *ET* [25]. Over the last few decades,
63 different physical and empirical remote sensing based models, which vary in complexity,
64 accuracy, and needing for ancillary metrological data, have been proposed for estimating *ET* at
65 different scales. In general, Accuracy in estimating *ET* basically depend on the accuracy of the
66 input satellite data products, such as land surface temperature (*LST*), normalized difference
67 vegetation index (*NDVI*), surface emissivity (ε_s) and surface albedo (α). However, the satellite
68 derived variables are in turn and it depend on factors relating to residual atmospheric effects,
69 spatial and temporal resolution, viewing angles, etc. Ancillary surface and atmospheric data like
70 wind speed, aerodynamic resistance, and surface roughness, which cannot readily be measured
71 through remote sensing techniques, usually required for these models. Therefore, it is still
72 challenging to estimate and produce *ET* maps at regional and even global scale using satellite
73 remote sensing without ground measurements or reanalyzed meteorological data. In order to
74 overcome this problem, some attempts have been made to develop new parameterizations for *ET*
75 estimation that depend entirely on remote sensing [30]. One widely used approach among them
76 is the *LST-NDVI* triangle method, which was proposed by [19-20] and improved by [21]. Briefly,
77 this method shows the relationship and the incident interaction between the soil, vegetation and
78 weather conditions. The *NDVI* values refer to the land cover type while, *LST* is a function in
79 weather conditions and soil moisture content. This method is based on the *P–T* (Priestley–
80 Taylor) equation [32], which can be considered as a simplified version of the more general
81 Penman equation [31]. The most sensitive point in this approach is the determination of ϕ which
82 substituted for the *P–T* parameter and accounts for aerodynamic and canopy resistances and
83 ranges from 0 at no *ET* to 1.26 at maximum *ET*. The ϕ parameter is estimated from the triangular
84 shape of the *LST-NDVI* feature space, which is formed by the scatterplot of *LST* versus *NDVI*
85 over a wide range of soil moisture content and fractional vegetation cover. The formalization of
86 the triangular shape is caused primarily by different sensitivity of *LST* to soil moisture variations
87 over bare soil and vegetated areas. There are several studies replaced the *NDVI* with other
88 Vegetation Indices (*VI*) such as fractional vegetation cover (*Fr*) [24-38] or broadband surface

89 albedo [41]. The advantages of *LST–VI* triangle method versus the other methods of surface
90 energy balance for estimating *ET* are that:- 1) very high accuracy in *LST* retrieval and
91 atmospheric correction are not indispensable, 2) needless to parameterize the complex
92 aerodynamic resistance and uncertainty originated from replacement of aerodynamic temperature
93 with *LST* is by passed, 3) it depends completely on remotely sensed *LST* and *VI*, 4) a direct
94 calculation of evaporative fraction (*EF*), and 5) estimations of the Evaporative Fraction (*EF)* and
95 the Net Radiation (*Rn)* are independent from each other. Therefore, the overall errors in *ET* can
96 be traced back to *EF* and *Rn* separately. There are some other methods making the estimation of
97 *EF* and *Rn* dependent on each other [3-29], thus making it impossible to trace errors separately.
98 Limitations of *LST–VI* triangle mainly lie in a bit subjective determination of both dry and wet
99 edges and a large number of pixels required over a flat area with a wide range of soil moisture
100 and fractional vegetation cover [38]. The triangle method has been applied successfully in certain
101 applications for estimation of both *ET* [13-20-28-33-34-35] and soil moisture [7-37]. The main
102 objective of this study is estimating daily ET_a directly with no need to estimate the net radiation
103 (*Rn*) and evaporative fraction (*EF*) instantaneously by using a simplified approach during the
104 winter agriculture season in the different growth stages of the crops cultivated in the study area.
105
106 **2.   Materials and Methods**

107 **2.1 Study area description**

108 El-Salhia project is located at the eastern part from Nile Delta as shown in (Fig. 1) and its
109 climate is dry arid according to Köppen Climate Classification System. The whole area of the
110 project is about 13,800 ha. Two irrigation systems are used in the project; the sprinkler irrigation
111 center pivot and the drip irrigation. The project has about 100 center pivot irrigation units. Each
112 pivot unit irrigates an area of about 63.6 ha. The common pivots length in the project is about
113 450 meter.

114
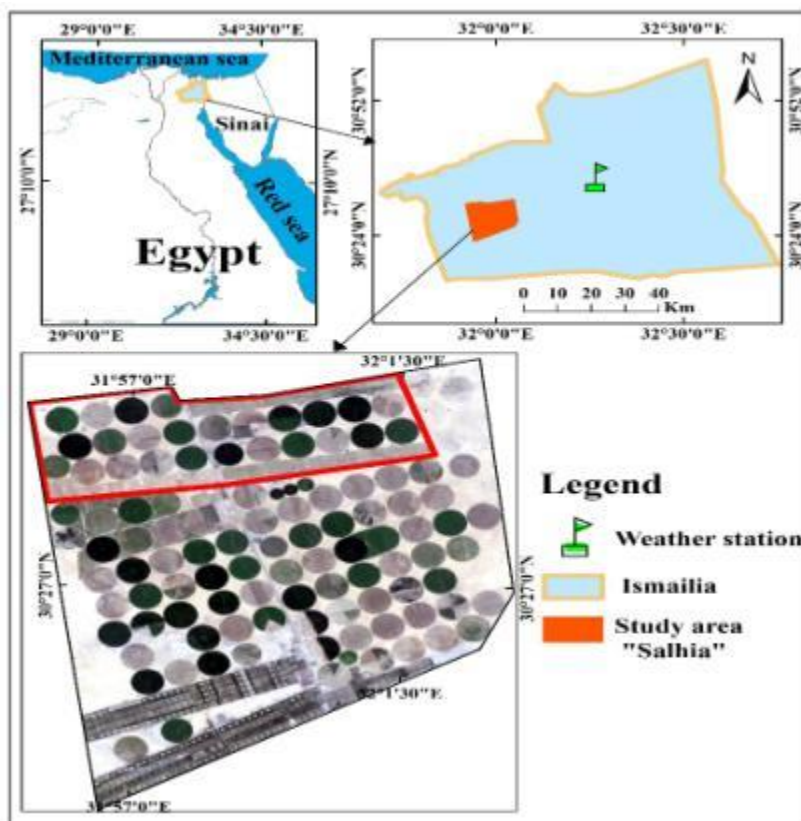
115   (Figure 1) Location map of the study area " Salhia".

116 **2.2   Data availability**

117 **Satellite data:** a combination of Landsat 7 and Landsat 8 (Path = 176 and Row = 39) were used
118 to cover winter season crops. Table (1) illustrates the details of Landsat 7 and 8 satellite data.
119   Table (1) illustrates the Landsat 7 and 8 satellite data details.

No.	Date	Sensor type	Spatial resolution	Number of bands
1	17-12-2013	Landsat 7		8
2	02-01-2014	Landsat 7	30m×30m	8
3	11-02-2014	Landsat 8		11
4	15-03-2014	Landsat 8		11
5	31-03-2014	Landsat 8		11
6	16-04-2014	Landsat 8		11
7	02-05-2014	Landsat 8		11

120 **Climatic metrological data:** ground meteorological data namely air temperature, wind speed,
121 dew point temperature and net radiation was used in order to calculate reference
122 evapotranspiration (*ETo*) during the days of the study.

123

124 **2.3 ET_a estimation**

125 The method applied here aimed to estimate daily ET_a directly by using the daily component of
126 the energy balance equation eq.1;

127                                      $$Rn = G + H + \lambda E   (1)$$

128 Where; R_n is net radiation (Wm^{-2}), G is the soil heat flux (Wm^{-2}), H is the sensible heat flux
129 (Wm^{-2}) and λE is the latent heat flux that is associated with the actual ET (Wm^{-2}). The energy
130 balance can be rewritten to;

$$\lambda E = EF \cdot (Rn - G) \qquad (2)$$

133 Where; EF is the dimensionless evaporative fraction and $(Rn - G)$ equals the net available
134 energy for ET. G can often be ignored for time scales of 1 day or more, and thus λE is a function
135 of Rn and EF only [42]. The EF is also defined as the ratio of actual ET to the available energy
136 (dimensionless).

$$EF = \frac{\lambda E}{Rn - G} \qquad (3)$$

138 The common formula which represents the Triangle method (Priestley and Taylor, 1972) was
139 used in this study according to (Priestley–Taylor) equation;

$$\lambda E = \phi[(Rn - G)\frac{\Delta}{\Delta+\gamma}] \qquad (4)$$

141 Where; ϕ is a substituted for P–T parameter, Δ is the slope of saturated vapor pressure at the air
142 temperature (kPa/K) and γ is the psychometric constant (kPa/K) and from eq. 2, 3 and 4, EF can
143 be rewritten as;

$$EF = \frac{\lambda E}{Rn - G} = \phi\left(\frac{\Delta}{\Delta+\gamma}\right) \qquad (5)$$

145 LST–VI triangle method (Fig. 2) was applied in this study in order to estimate ϕ parameter. It is
146 originated from the parameterization of [19], in a simplified P–T formula [32]. Regional ET_a and
147 EF were estimated according to Eq. (4) which depends almost completely on remotely sensed
148 data. The accurate interpreting of the scatter plot which resulted from remotely sensed LST and
149 $NDVI$ under conditions of variance ranges of soil moisture availability and vegetation cover
150 leads to accurate estimation of regional ET_a.

151
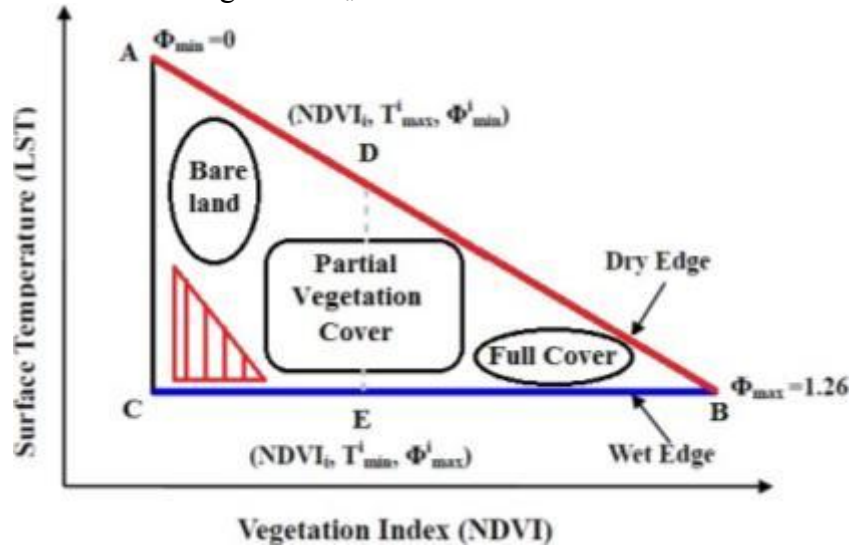
152 (Fig.2) Schematic diagram interpret the scatter plot of (LST–$NDVI$) triangular space to estimate
153 evaporative fraction using wet and dry surfaces assumption and data distribution entire the triangle.
154

155 The dry edge is the oblique red solid line (*AB*) and the wet edge is the horizontal blue solid line
156 (*CB*) represent the minimum *ET* and maximum *ET*, respectively. The two boundaries (dry and
157 wet edges) of the *LST-NDVI* feature space represent limiting conditions for the surface fluxes.
158 These edges respectively represent two limiting cases of soil moisture content and so evaporative
159 fraction for each *NDVI* value (i.e., the unavailability of soil moisture and stressed vegetation at
160 the dry edge and non-stressed vegetation which evaporate potential *ET* at the wet edge).
161 Specifically, EF at the wet edgy is EF_{max} ($EF_{max}=1$) so, pixels at the wet edge are regarded to
162 evaporate/transpirate potentially while at the dry edge, EF varies from EF_{min} ($EF_{min}=0$) at the dry
163 bare soil to EF_{max} ($EF_{max}=1$) at fully non stressed vegetation cover when availability of root zone
164 soil water is good. At the dry edge, ET_a mainly comes from the transpiration of vegetation from
165 the root zone water as the soil surface hasn't enough water to evaporate. The values of (ϕ) also
166 ranges from ($\phi_{min} = 0$) at dry bare soil pixels to ($\phi_{max} =1.26$) at non stressed with full vegetation
167 cover pixels and the other ϕ values for each pixel are based on its soil water content and partial
168 vegetation cover. In the absence of significant advection and convection, ϕ in eq. (4 and 5) can
169 take a wider range of 0 (no *ET*) to $\left(\frac{\Delta+\gamma}{\Delta}\right)$ (maximum *ET*).
170 Determination of dry and wet edges in the *LST–NDVI* scatter is necessary, to estimate pixel by
171 pixel *ET* and *EF* using Eqs. (4) and (5). In arid and semi-arid areas, it should be noted that, for
172 given vegetation cover, spatial pixels with high surface temperature and low *EF* are detectable
173 by satellite remote sensors. On the other hand, the saturated soil water which evaporates
174 potentially pixels is rarely and hardly existed in these conditions (see red lined triangle inside
175 fig.2).
176 Obtaining of the ϕ value for each pixel requires a three step linear interpolation scheme based on
177 the *LST-NDVI* triangle which used to allocate ϕ values inside the scatterplot (Fig. 2); (1)
178 determines the dry and wet edges in the triangular space. The *EF* estimation accuracy depends
179 basically on the accuracy of determining wet and dry edges; (2) minimum and maximum ϕ are
180 respectively set to $\phi min = 0$ for the driest bare soil pixel "with lowest *NDVI* and highest *LST*"
181 (point A) and $\phi max = 1.26$ for the full vegetated pixel "with largest *NDVI* and lowest *LST*"
182 (point B). For each $NDVI_i$ value, there are max and min values of ϕi, ϕi_{max} located on the wet
183 edge (point E) (ϕi_{max} is generally set to $\phi i_{max} = \phi_{max} = 1.26$) and ϕi_{min} Located on the dry edge
184 (point D). 3) Finally, ϕi entire each *NDVI* value, is linearly interpolated between ϕi_{min} and ϕi
185 $_{max}$ through the similarity between the *ABC* and *EBD* triangles (Fig. 2). The following relation is
186 taking out from the similarity;

$$\frac{AD}{AB} = \frac{ED}{AC}$$

187 Thus, by converting the symbols into real parameters, ϕ value for each pixel can be calculated
188 using the given mathematical expression as follows;

189
190 $$\phi i = [(\frac{Tmax-Ti}{Tmax-Tmin})*(\phi max -\phi min)] + \phi min \qquad (6)$$
191

192 Since the ϕ_{min} is equal to zero and ϕ_{max} is equal to 1.26, the eq.6 becomes as:
193

194 $$\phi i = (\frac{Tmax-Ti}{Tmax-Tmin})*1.26 \qquad (7)$$

195
196 The above scheme accuracy depend on the accurate determination of the dry and wet edges, as
197 the eq.7 depends on T_{max} which represents the high value on the dry edge and T_{min} which

198   represents the wet edge as optimal conditions for *ET*. Also, intensive care during the pre-
199   processing and extracting the *LST* from the remote sensing data must be taken into account.
200   (Fig.3) represents of the relation between *LST* and *NDVI* for sample of our data which illustrates
201   the triangle shape and both of dry edge (oblique red line) and wet edge (horizontal blue line).

202
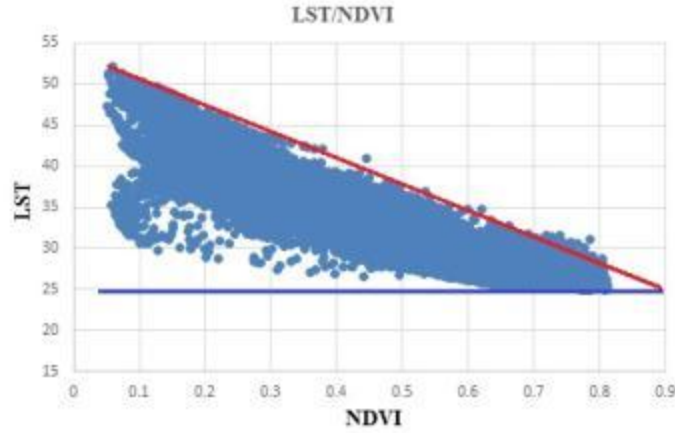
203   (Fig.3) Scatterplot which illustrates the triangle shape and both of dry edge (oblique red line) and
204   wet edge (horizontal blue line).

205

206   Daily (24 hours) R_n according was estimated by using the [3] equation as [1] and [9] used the
207   following equation to calculate it;

$$R_{n24} = (1-\alpha)Rs_{\downarrow}-110\tau_{sw24} \quad (8)$$

208

209   Where; R_{n24} is the daily net radiation (wm^{-2}), α is the surface albedo, $Rs_{\downarrow}$ is the 24hour solar
210   radiation (wm^{-2}) and τ_{sw24} is the atmospheric transmissivity.

211   The following assumption was used to estimate daily *ET* values in a direct way; the near noon
212   instantaneous *EF*, which estimated by the triangle method was used as a representative value to
213   the daily average *EF* value based on the observations of [6-8] for both homogeneous and
214   heterogeneous land surfaces EF remains fairly constant for daylight hours, particularly at about
215   10:00 and 16:00 O'clock and this assumption used by [30]. During daytime, *EF* is mainly
216   controlled and determined by land surface properties such as vegetation amount, soil moisture
217   and surface resistance to heat and momentum transfer. Most of them are slowly varying
218   parameters during daytime as compared to other fast changing variables (e.g., surface
219   temperature and radiation), which have much stronger diurnal cycles due to radiation and
220   atmospheric forcing [22]. On the other hand, analysis of our hourly climate data showed that the
221   difference between meteorological parameters such as air temperatures and relative humidity at
222   the satellite overpass time and the daily average of these parameters were not considerable. The
223   highest relative error value of air temperature and relative humidity values during the overpass
224   time value and the average daily value was not exceed 9.8% and 15% respectively over the seven
225   used dates of data. Hence, we can regard the weather conditions during the satellite overpass
226   time are representative of the whole day and *EF* too. In addition to, several studies have
227   concluded that using local near noon *EF* instead of daily *EF* for daily *ET* estimation incurs very
228   small error [14-15-16-18].

229

$$ET_{daily} = (R_{n\,daily} - G_{\,daily}) * EF_{\,daily} \quad (9)$$

230

231 As the daily G ignored in this study, as it is usually assumed negligible over the diurnal cycle or
232 day time scale [12-22-36-38]. The above equation can be rewritten as;

233
234
$$ET_{daily} = (R_{n\,daily} * EF_{daily}).\qquad(10)$$

235 **2.4 Validation strategy.**

236 Crop Evapotranspiration (ETc) has been used to chick the performance and the results of the
237 proposed procedure by converting it from ETc to actual ET_a using the crop water stress index
238 ($CWSI$) extracted from satellite images. ETc calculated by multiplying FAO table crop
239 coefficient (Kc) and reference evapotranspiration ETo. There are many different approaches used
240 for estimating reference ETo such as Penmamn-Monteith, Blaney-Criddle and Hargreaves
241 Samani [30-31]. Here, we used the FAO-Penmamn-Monteith (FPM) equation to calculate the
242 ETo. The $CWSI$ is based on observed canopy-air temperature differences and is an index for the
243 water availability in the soil. When a crop with full cover has adequate water it will transpire at
244 the potential rate for that crop. The actual evapotranspiration ET_a rate will fall below the
245 potential rate when water becomes limiting [4-5-17-23]. The $CWSI$ ranges from 0 (no stress) to 1
246 (maximum stress) and has been defined as:

247
$$CWSI = 1 - (ET_a/ET_c)\qquad(11)$$

248 The following expression used to calculate CWSI as a function in difference in LST.

249
$$CWSI = \frac{(Ti - Tmin)}{(Tmax - Tmin)}\qquad(12)$$

250 Where; T_i is the LST of each pixel, T_{min} is the minimum LST, T_{max} is the maximum LST at the
251 study area. This strategy was applied to verify the accuracy of the results of this approach on the
252 wheat, potato and sugar beet crops during the different growth stages.

253 **3. Results and Discussions**

254 Daily ET_a was calculated by using eq.10, which consist of two main components EF and Rn. EF
255 estimated by triangle method, which parameterize (P-T) parameter from the $LST/NDVI$ scatter
256 plot. The parameter (ϕ) is a down samples coefficient for both aerodynamic and surface
257 resistance of evaporation and making the complicated sensible heat calculations are not needed
258 the thing which make this procedure is more simple than others models. The (ϕ) parameter
259 basically depends on and estimated by using LST in a form of rational equation which eliminates
260 the error in LST calculation "if there is error". There are other parameters in eq.5 which entered
261 in calculation of EF such as Δ and γ which depend on air temperature. In this study, we used the
262 air temperature which obtained from the metrological station in order to calculate the Δ and γ,
263 but there are many studies aimed at correlate the LST and T_{air} in order to dispense of
264 metrological information completely. The second component is the net radiation Rn, which
265 estimated by using eq.8 at daily scale directly rather than instantaneous calculations. ETa
266 estimated by the proposed procedure validated against actual ET_a adjusted from ETc by using the
267 $CWSI$ which account for the soil moisture availability. Wheat, potato and sugar beet are three
268 herbaceous crops which were used to test the validity of this procedure. The results showed high
269 agreement and responsible results during different growth stages over these crops. The R^2 values
270 of wheat, potato and sugar beet were 0.88, 0.98 and 0.99 respectively which mean that the
271 proposed procedure had enough accuracy for wheat, potato and sugar beet at least in our case.
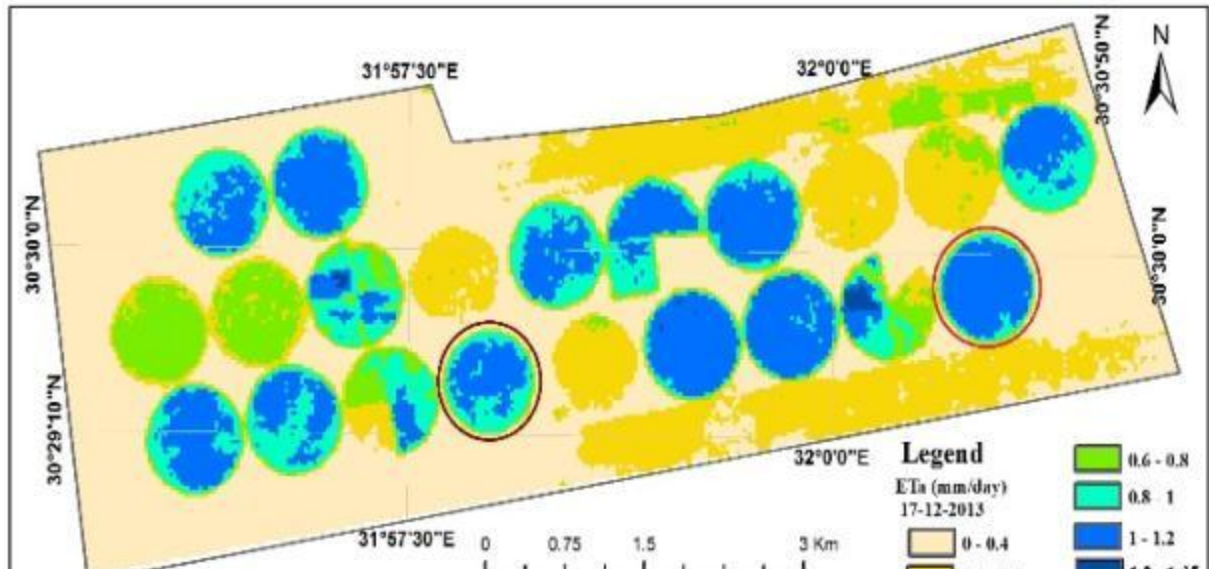
WHEAT

POTATO

SUGAR BEET

272

273

274
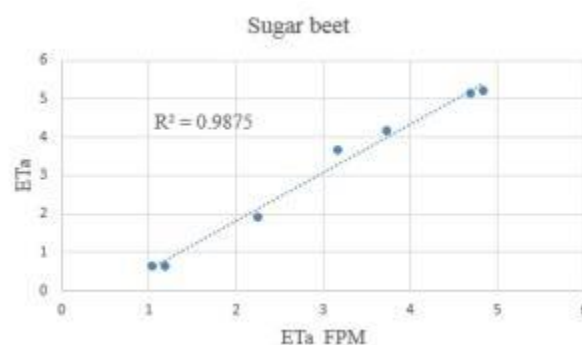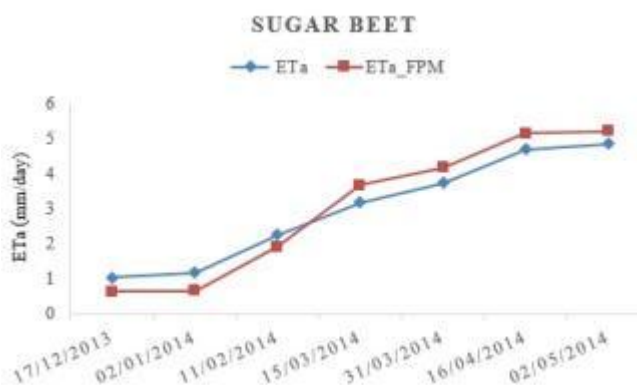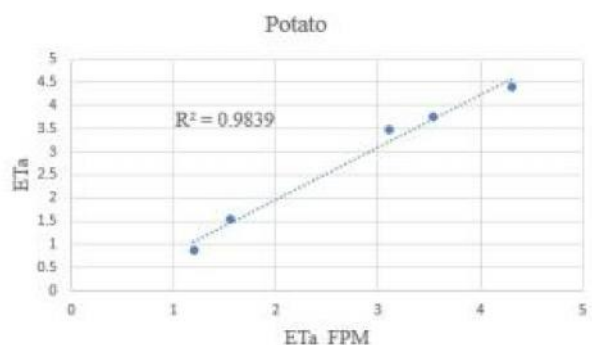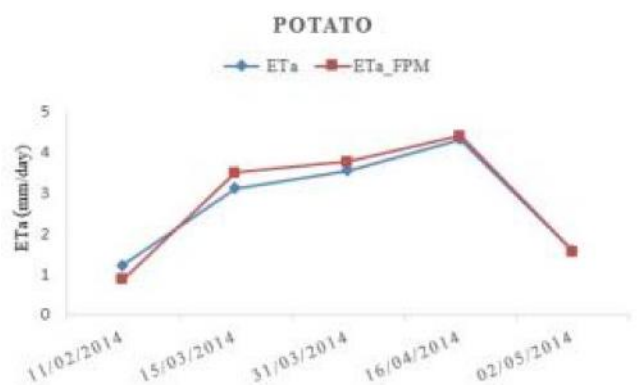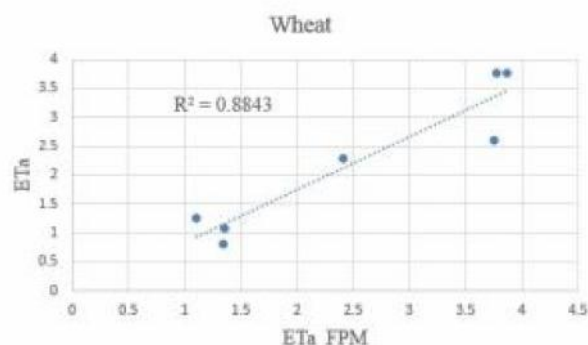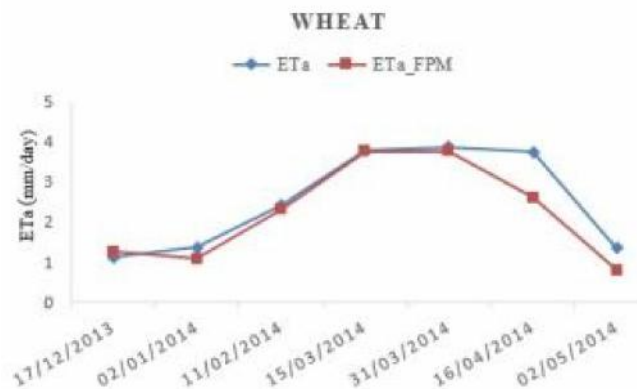
(Fig.4) shows matching and the correlation between actual evapotranspiration ETa estimated by the triangle method and the actual evapotranspiration (ETa_FPM) adjusted from FAO-Penmamn-Monteith (FPM) crop evapotranspiration ETc by using the crop water stress approach for many crops cultivated in the study area during different growth stages

Maps of daily *ETa* were created for all study area crops but for better view, we viewed a part which contains the studied center pivot units of the different crops in fig.5 and detailed ETa distribution for these crops (wheat, potato and sugar beet) at different crop stages in fig.6. The highlighted red, purple and brown circles represent wheat, potato and sugar beet respectively. In 17th of December the *ETa* values for wheat and sugar beet were 1.1 and 1 *mm/day* respectively and the validation values for these crops at the same date were 1.24 and 0.63 *mm/day* respectively. These values showed good agreement as the wheat and sugar beet where the RMSE were 0.101 and 0.277 respectively. In 2nd of January, the *ETa* values for wheat and sugar beet were 1.35 and 1.17 *mm/day* respectively and the validation values for these crops at the same

date were 1.07 and 0.65 *mm/day* respectively. These values showed good agreement as the wheat and sugar beet where the RMSE were 0.201 and 0.37 respectively. In 11th of February, the *ETa* values for wheat, potato and sugar beet were 2.41, 1.2 and 2.25 *mm/day* respectively and the validation values for these crops at the same date were 2.29, 0.86 and 1.9 *mm/day* respectively. These values showed good agreement as the wheat, potato and sugar beet where the RMSE were 0.079, 0.23 and 0.24 respectively. In 15th of March, the *ETa* values for wheat, potato and sugar beet were 3.78, 3.1 and 3.16 *mm/day* respectively and the validation values for these crops were 3.76, 3.48 and 3.67 *mm/day* respectively. These values showed good agreement as the wheat, potato and sugar beet where the RMSE were 0.013, 0.26 and 0.36 respectively. In 31th of March, the ETa values for wheat, potato and sugar beet were 3.87, 3.54 and 3.72 *mm/day* respectively and the validation values for these crops at the same date were 3.75, 3.75 and 4.16 *mm/day* respectively. These values showed good agreement as the wheat, potato and sugar beet where the RMSE were 0.079, 0.15 and 0.31 respectively. In 16th of April, the *ETa* values for wheat, potato and sugar beet were 3.75, 4.3 and 4.66 *mm/day* respectively and the validation values for these crops at the same date were 2.6, 4.4 and 5.14 *mm/day* respectively. These values showed good agreement for potato and sugar beet where the RMSE were 0.06 and 0.32 respectively, but for wheat there was significant error as the RMSE was 0.81. In 2nd of May, the *ETa* values for wheat, potato and sugar beet were 1.3, 1.55 and 4.83 *mm/day* respectively and the validation values for these crops at the same date were 0.8, 1.55 and 5.2 *mm/day* respectively. These values showed good agreement as the wheat, potato and sugar beet where the RMSE were 0.38, 0.004 and 0.25 respectively. For crop wheat, there were no significant error at the initial development and mid stages, but at the late stage a high significant error appeared as the RMSE were 0.81 in 16th of April and 0.38 in 2nd of May. We interpreted the significant error at the late stage to many reason: 1) at the late stage wheat leaves, especially basal leaves, became almost dead which mean that the cell structure is more weak and able to water absorption than healthy leaves (development and mid stages). 2) sprinkler irrigation system increase the leaves water absorption chance. 3) Continuation of the irrigation process to later stages every day or at least day after day. The previous reasons made the LST and surface albedo (α) down normal, the thing which raise the EF and Rn values respectively. Rising of EF and Rn values led to raising of estimated ETa value. Absence of this significant error with potato and sugar beet "ever green until harvest crops" support our interpretation. This mean that the proposed method need to test for wheat under other irrigation systems like surface or drip irrigation.
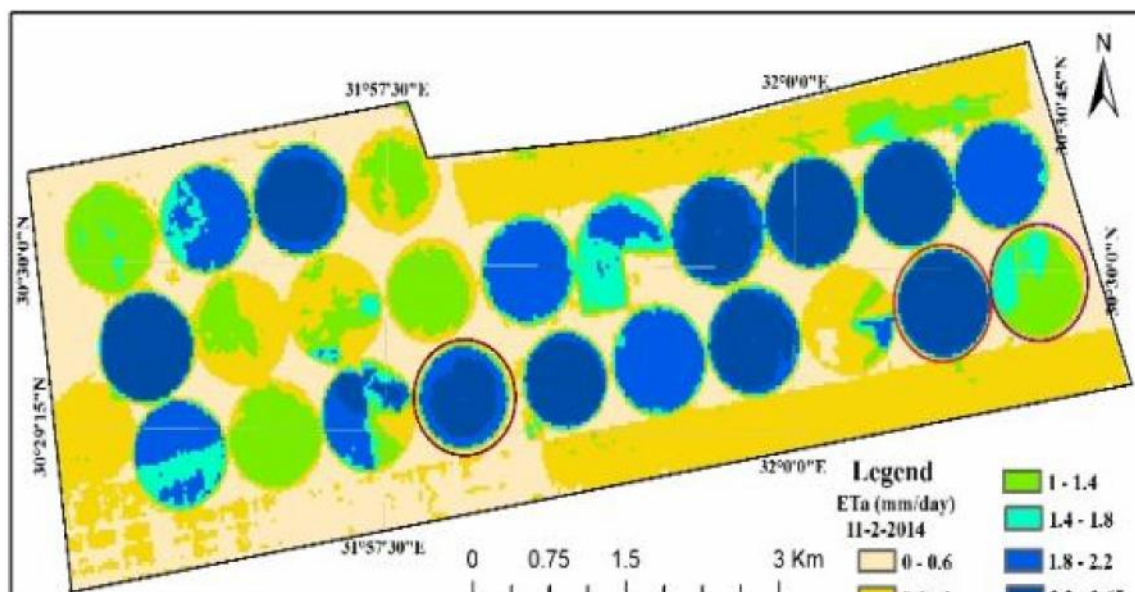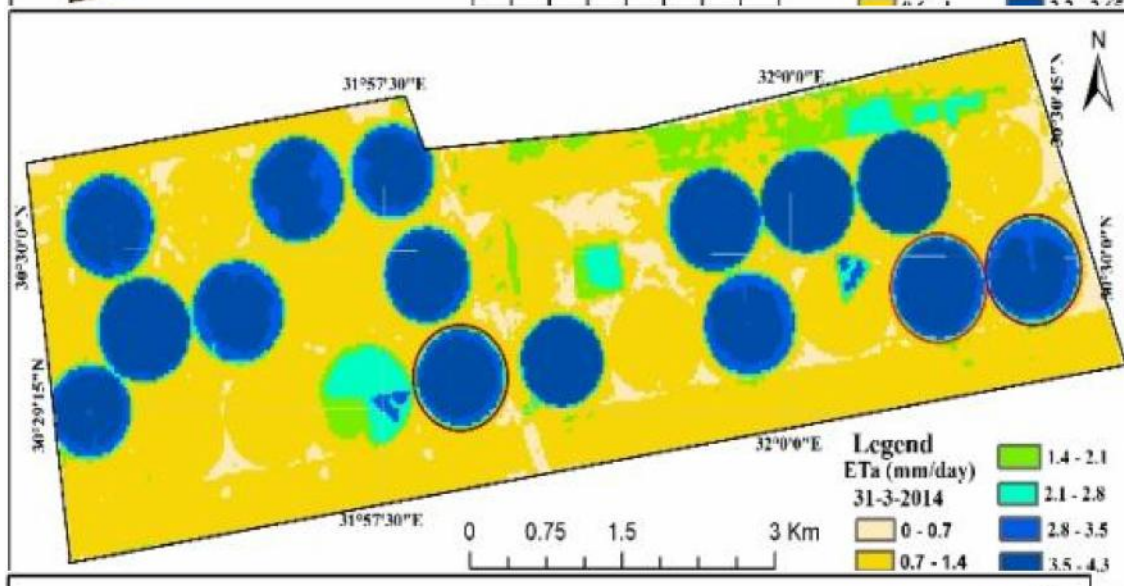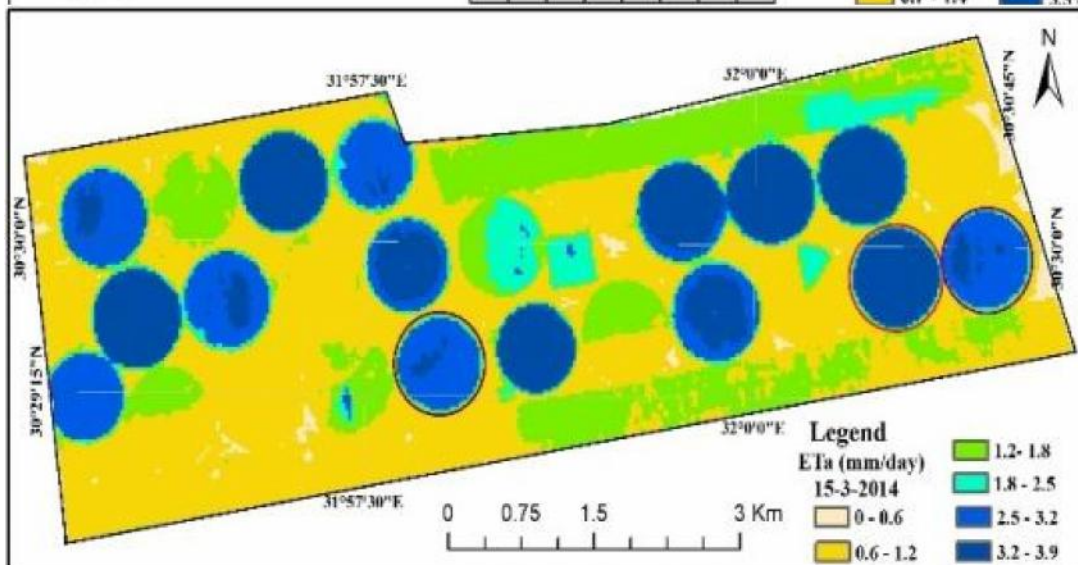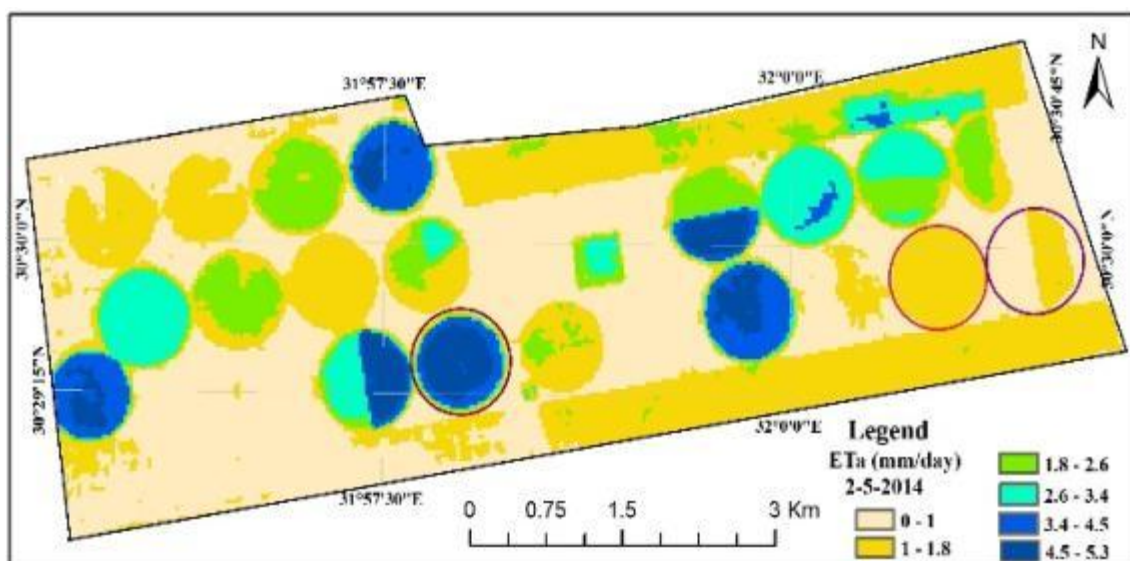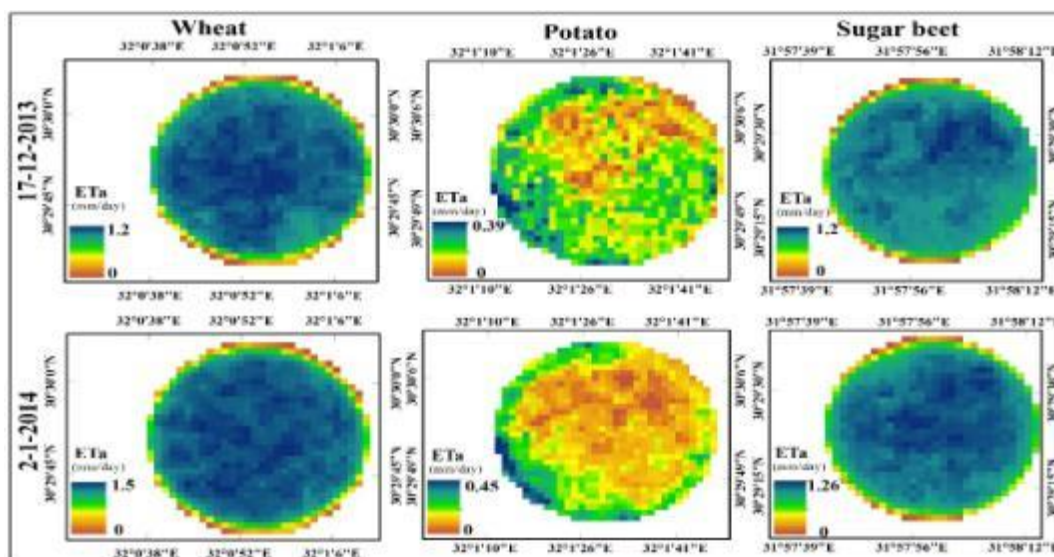
320

321

322
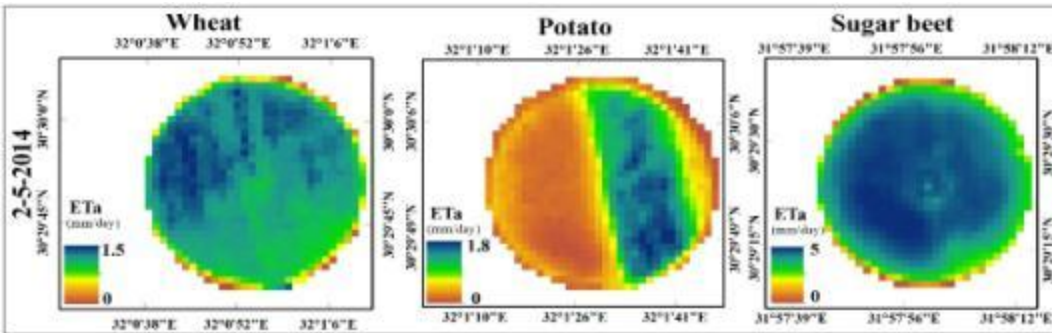
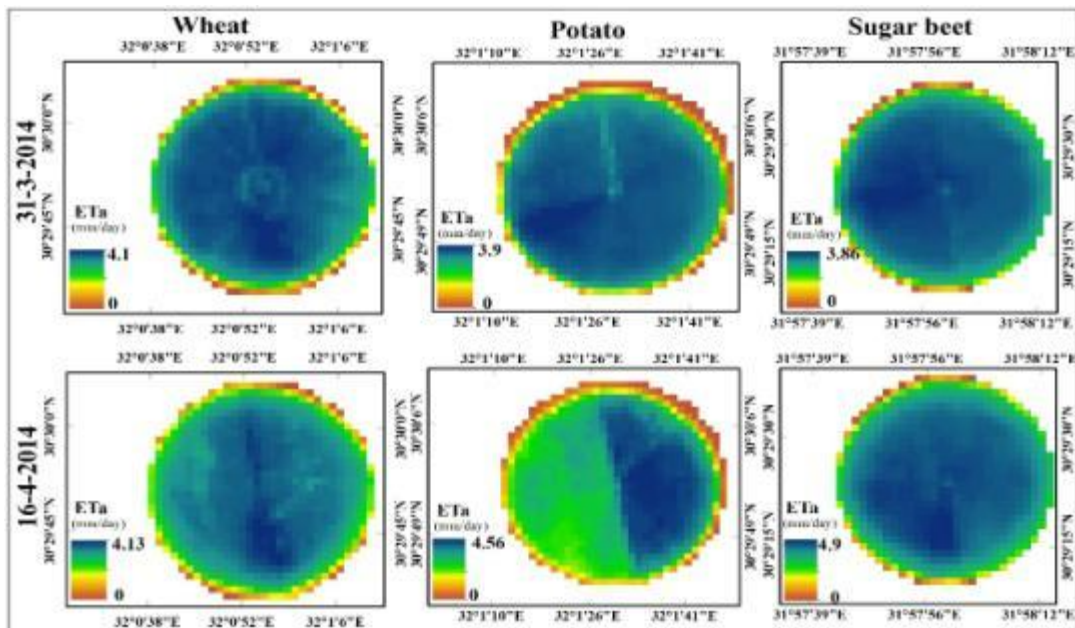323
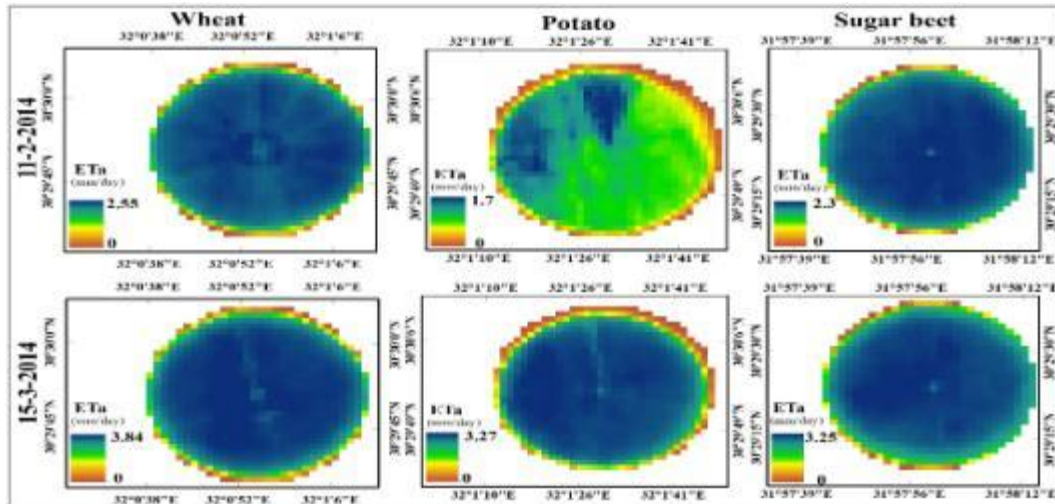
324

325

326
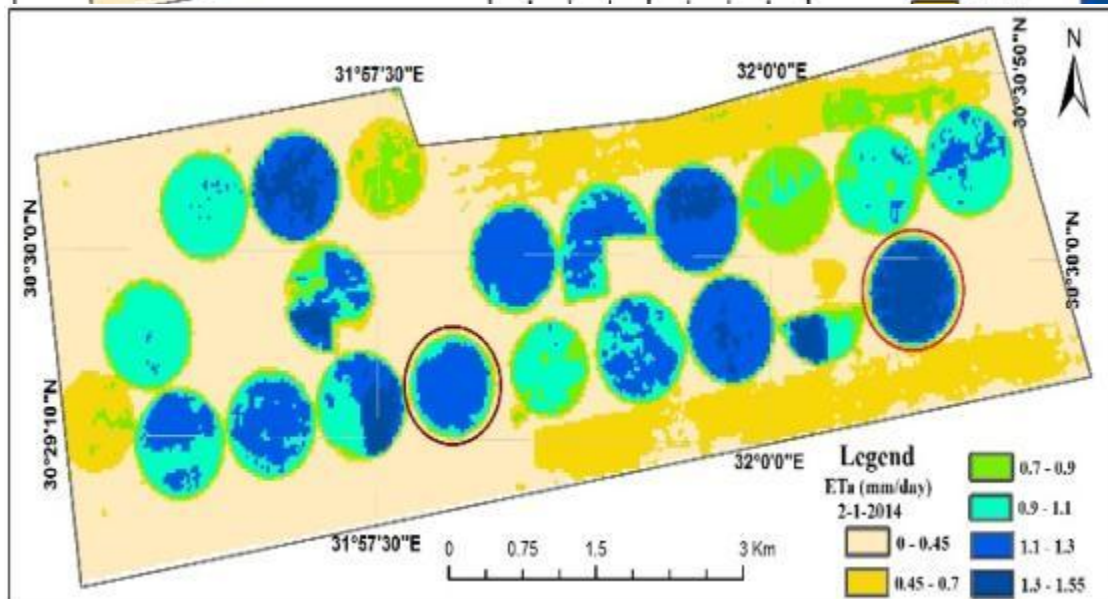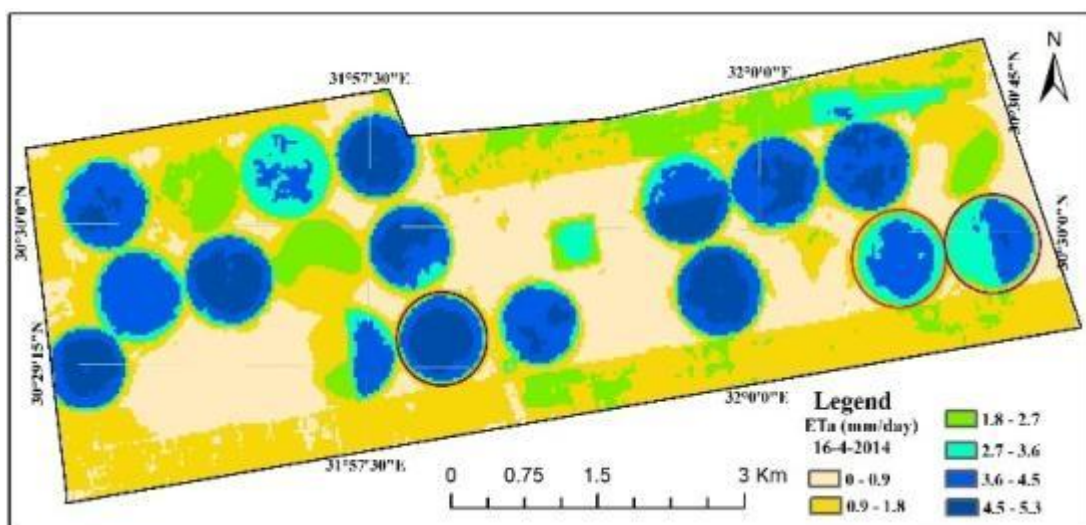
327 (Fig.5) distribution of daily ETa over different crops developing stages during the winter season.

328

329

330

331

332   (Fig.6) ETₐ distribution for wheat, potato and sugar beet crops which used for validation during
333   different crop stages. (Note: on 17th of December, 2013 and 2nd of January, 2014, the potato
334   Pivot was not cultivated)

335

4. Conclusion

Decision-makers and water resources managers are always need to regional information about *ET* to manage water resources distribution. Triangle remote sensing method was proposed by [19-20] and improved by [21]. This method is used for estimating spatial distributed regional *ET* and soil moisture content. Although, this method estimates instantaneous value of Evaporative Fraction (EF), it could be used to estimate daily *ETa* directly; the near noon instantaneous *EF*, which estimated by the triangle method is used as a representative value to the daily average *EF* value which strengthened by the analysis of our climatic data. Actual *ET* at daily scale had been estimated directly for different dates during the winter season over different crops cultivated there. The assessment strategy conducted on three crops, wheat, potato and sugar beet through a comparison between *ETa* estimated by the proposed procedure and *ETa* adjusted from *ETc* using the *CWSI* approach. ETc calculated by using of ET_o from FAO Penman-Monteith (FPM) equation and FAO crop coefficient (KC). The ET_a values of wheat varied from 1.1 mm/day at the development stage to 3.78 mm/day at the mid stage as the highest value, then 1.3 mm/day at the late stage. Potato graduated from 1.2 mm/day at the initial stage to 4.3 mm/day at the mid stage as the highest value, then 1.55 mm/day at the late stage. The last crop is sugar beet which graduated from 1 mm/day at the initial stage to 4.83 mm/day at the mid stage. The maximum RMSE for the wheat (before the late season), potato and sugar beet is 0.20, 0.26 and 0.37 respectively over the different dates. At the late stage of wheat a high significant error appears due to the sprinkler irrigation system effect on the mature wheat. The results showed high agreement between the two methods values during the growing season of the three crops. The R^2 values were 0.88, 0.98 and 0.99 for wheat, potato and sugar beet respectively which mean that, this method is a responsible, realistic and acceptable for estimating daily ET_a at regional scale. We recommend that, the proposed method need to evaluate for wheat under other irrigation systems rather than sprinkler irrigation system.

5. Reference

1. Allen RG, Tasumi M, Mores A, Bastiaanssen WGM, Kramber WJ, Anderson H N. Evapotranspiration from landsat (SEBAL): Application in the U.S., proceedings of Annual Conference of the International Commission on Irrigation and Drainage, Seoul, Korea. 2001.
2. Anderson MC, Allen RG, Morse A, Kustas WP. Use of Landsat thermal imagery in monitoring evapotranspiration and managing water resources. Remote Sensing of Environment. 2012; 122: 50-65.
3. Bastiaanssen WGM. SEBAL-based sensible and latent heat fluxes in the irrigated Gediz Basin, Turkey. J Hydrol (Amst). 2000; 229:87–100. doi:10.1016/S0022-1694(99)00202-4.
4. Boegh E, Soegaard H, Thomsen A. Evaluating evapotranspiration rates and surface conditions using Landsat TM to estimate atmospheric resistance and surface resistance. Remote Sens Environ. 2002; 79:329–343. doi:10.1016/S0034-4257(01)00283-8.
5. Boulet G, Chehbouni A, Gentine P, Duchemin B, Ezzahar J, Hadria R. Monitoring water stress using time series of observed to unstressed surface temperature difference. Agric For Meteorol. 2007; 146(3–4):159–172.

6. Caparrini F, Castelli F, Entekhabi D. Estimation of Surface Turbulent Fluxes through Assimilation of Radiometric Surface Temperature Sequences, J. Hydrometeorol. 2004; 5: 145–159.

7. Carlson TN, Gillies RR, Schmugge TJ. An interpretation of methodologies for indirect measurement of soil water content. Agric For Meteorol. 1995b; 77:191–205.

8. Crago R D. Conservation and variability of the evaporative fraction during the daytime, J. Hydrol. 1996; 180:173–194.

9. De Bruin HAR, Stricker JNM. Evaporation of grass under non-restricted soil moisture conditions. Hydrol. Sci. J. 2000;45:391‑406.

10. Droogers P, Immerzeel WW, Lorite IJ. Estimating actual irrigation application by remotely sensed evapotranspiration observations. Agricultural Water Management. 2010; 97:1351–1359.

11. Er-Raki S, Chehbouni A, Guemouria N, Duchemin B, Ezzahar J, Hadria R. Combining FAO-56 model and ground-based remote sensing to estimate water consumptions of wheat crops in a semi-arid region. agricultural water management. 2007; 87: 41–54.

12. Galleguillos M, Jacob F, Pr´evot L, French A, Lagacherie P. Comparison of two temperature differencing methods to estimate daily evapotranspiration over a Mediterranean vineyard watershed from ASTER data, Remote Sens. Environ. 2011; 115: 1326–1340.

13. Gillies RT, Carlson TN, Cui J, Kustas WP, Humes KS. A verification of the ''triangle'' method for obtaining surface soil water content and energy fluxes from remote measurements of the Normalized Difference Vegetation Index (NDVI) and surface radiant temperatures. Int J Remote Sens .1997; 18(15):3145–3166.

14. Farah H, Bastiaanssen W, Feddes R. Evaluation of the temporal variability of the evaporative fraction in a tropical watershed, Int. J. Appl. Earth Obs. Geoinf. 2004; 5:129–140.

15. Hall F G, Huemmrich K F, Goetz S J, Sellers P J, Nickeson J E. Satellite Remote Sensing of Surface Energy Balance: Success, Failures, and Unresolved Issues in FIFE, J. Geophys. Res. 1992; 97:19061–19089, doi:10.1029/92jd02189.

16. Hoedjes J, Chehbouni A, Jacob F, Ezzahar J, Boulet G. Deriving daily evapotranspiration from remotely sensed instantaneous evaporative fraction over olive orchard in semi-arid Morocco, J. Hydrol. 2008; 354:53–64.

17. Jackson RD, Idso SB, Reginato RJ, Pinter PJ. Canopy temperature as a crop water stress indicator.Water Resour Res. 1981; 17:1133–1138.

18. Jia L, Xi G, Liu S, Huang C, Yan Y, Liu G. Regional estimation of daily to annual regional evapotranspiration with MODIS data in the Yellow River Delta wetland, Hydrol. Earth Syst. Sci. 2009; 13:1775–1787.

19. Jiang L, Islam S. A methodology for estimation of surface evapotranspiration over large areas using remote sensing observations. Geophysical Research Letters. 1999; 26: 2773‑2776.

20. Jiang L, Islam S. Estimation of surface evaporation map over southern Great Plains using remote sensing data. Water Resour Res. 2001; 37:329–340.

21. Jiang L, Islam S. An intercomparison of regional latent heat flux estimation using remote sensing data. International Journal of Remote Sensing. 2003; 24:2221‑2236.

22. Jiang L, Islam S, Guo W, Jutla A, Senarath S, Ramsay H, Eltahir E. A satellite-based daily actual evapotranspiration estimation algorithm over South Florida. Global and Planetary Change. 2009; 67:62–77.

23. Kustas WP, French AN, Hatfield JL, Jackson TJ, Moran MS, Rango A. Remote sensing research in hydrometeorology. Photogramm Eng Remote Sensing. 2003a; 69(6):613–646.

24. Liang S, Rui S, Xiaowen L, Huailiang c, Xuefen Z. Estimating Evapotranspiration Using Improved Fractional Vegetation Cover and Land Surface Temperature Space. Journal of Resources and Ecology. 2011; 2(3): 225-231.

25. Li X, Lu L, Yang W, Cheng G. Estimation of evapotranspiration in an arid region by remote sensing—A case study in the middle reaches of the Heihe River Basin. International Journal of Applied Earth Observation and Geoinformation. 2012; 17:85–93.

26. Martha C A, Richard G A, Anthony M, William P K. Use of Landsat thermal imagery in monitoring evapotranspiration and managing water resources. Remote Sensing of Environment. 2012; 122: 50–65.

27. Allam MN, Allam GI. Water Resources in Egypt:Future challeges and opportunities. International Water Resources Association Water International. 2007; 32 (2):205-218.

28. Nemani R, Running SW. Estimation of regional surface resistance to evapotranspiration from NDVI and thermal-IR AVHRR data. J Appl Meteorol. 1989; 28:276–284.

29. Norman JM, Kustas WP, Humes KS. A two-source approach for estimating soil and vegetation energy fluxes from observations of directional radiometric surface temperature. Agric For Meteorol. 1995; 77:263–293.

30. Pandey V, Pandey PK, Mahanta AP. Calibration and performance verification of Hargreaves Samani equation in a humid region. Irrig. Drain. 2014; 63:659–667. http://dx.doi.org/10.1002/ird.1874.

31. Pandey PK, Dabral PP, Pandey V. Evaluation of reference evapotranspiration methods for the northeastern region of India, International Soil and Water Conservation Research, http://dx.doi.org/10.1016/j.iswcr.2016.02.003

32. Peng J, Liu Y, Zhao X, Loew A. Estimation of evapotranspiration from MODIS TOA radiances in the Poyang Lake basin, China. Hydrol. Earth Syst. Sci. 2013; 17:1431–1444.

33. Penman HL. Natural evaporation from open water, bare soil and grass, P. Roy. Soc. London Ser. A. 1948; 193:120–145.

34. Priestley CHB, Taylor R J. On the assessment of surface heat flux and evaporation using large-scale parameters. Monthly weather review. 1972; 100:81−92.

35. Price JC. Using spatial context in satellite data to infer regional scale evapotranspiration. IEEE Transactions on Geoscience and Remote Sensing. 1990; 28:940–948.

36. Rasmussen MO, Sørensen MK, Wu B, Yan N, Qin H, Sandholt I. Regional-scale estimation of evapotranspiration for the North ChinaPlain using MODIS data and the triangle-approach. International Journal of Applied Earth Observation and Geoinformation. 2014; 31:143–153.

37. Roerink GJ, Su Z, Menenti M. S-SEBI: a simple remote sensing algorithm to estimate the surface energy balance. Phys Chem Earth, Part B Hydrol Oceans Atmos. 2000; 25(2):147–157.

38. S´anchez JM, Scavone G, Caselles V, Valor E, Copertino VA, Telesca V. Monitoring daily evapotranspiration at a regional scale from Landsat-TM and ETM+ data: Application to the Basilicata region, J. Hydrol. 2007; 351:58–70, doi:10.1016/j.jhydrol.2007.11.041, 2008.

39. Sandholt I, Ramussen K, Anderson J. A simple interpretation of surface temperature/vegetation index space for assessment of surface moisture status. Remote Sensing of Environment. 2002; 79:213–224.

40. Tang R, Li Z, Tang B. An application of the Ts−VI triangle method with enhanced edges determination for evapotranspiration estimation from MODIS data in arid and semi-arid regions: Implementation and validation. Remote Sensing of Environment. 2010; 114:540–551.

41. Wang K, Li Z, Cribb M. Estimation of evaporative fraction from a combination of day and night land surface temperatures and NDVI: A new method to determine the Priestley−Taylor parameter. Remote Sensing of Environment. 2006; 102:293–305.

42. Wang KC, Dickinson RE A review of global terrestrial evapotranspiration: Observation, modeling, climatology, and climatic variability. Reviews of Geophysics, 50, RG2005. 2012; http://dx.doi.org/10.1029/2011RG000373.

43. Yang J, Wang Y. Estimating evapotranspiration fraction by modeling two-dimensional space of NDVI/albedo and day−night land surface temperature difference: A comparative Study. Advances in Water Resources. 2011; 34:512–518.

44. Zwart SJ, Bastiaanssen WGM, Fraiture C, Molden DG. WATPRO: A remote sensing based model for mapping water productivity of wheat. Agricultural Water Management. 2010; 97: 1628–1636.